A Framework for Phasor Measurement Placement in Hybrid State Estimation Via Gauss–Newton

Xiao Li, *Student Member, IEEE*, Anna Scaglione, *Fellow, IEEE*, and Tsung-Hui Chang, *Member, IEEE*

***Abstract*—In this paper, we study the placement of phasor measurement units (PMU) for enhancing hybrid state estimation via the traditional Gauss-Newton method, which uses measurements from both PMU devices and Supervisory Control and Data Acquisition (SCADA) systems. To compare the impact of PMU placements, we introduce a useful metric which accounts for three important requirements in power system state estimation: *convergence*, *observability* and *performance* (COP). Our COP metric can be used to evaluate the estimation performance and numerical stability of the state estimator, which is later used to optimize the PMU locations. In particular, we cast the optimal placement problem in a unified formulation as a semi-definite program (SDP) with integer variables and constraints that guarantee observability in case of measurements loss. Last but not least, we propose a relaxation scheme of the original integer-constrained SDP with randomization techniques, which closely approximates the optimum deployment. Simulations of the IEEE-30 and 118 systems corroborate our analysis, showing that the proposed scheme improves the convergence of the state estimator, while maintaining optimal asymptotic performance.**

***Index Terms*—Convergence, estimation, optimal placement.**

I. Introduction

POWER SYSTEM state estimation (PSSE), using nonlinear power measurements from the Supervisory Control and Data Acquisition (SCADA) systems, is plagued by ambiguities and convergence issues. Today, the more advanced phasor measurement units (PMUs) deployed in wide-area measurement systems (WAMS) provide synchronized voltage and current phasor readings at each instrumented bus by leveraging the GPS timing information. PMUs data benefit greatly state estimation [2], because, if one were to use only PMUs, the state can be obtained as a simple linear least squares solution in one shot [3]. However, the estimation error can be quite high, and the system can lose even observability, due to the limited deployment of PMUs. For this reason, researchers have proposed hybrid state estimation schemes [4], integrating both PMU and SCADA data. Some of these methods incorporate the PMU measurements into the iterative state estimation updates [5]–[7], while others use PMU data to refine the estimates obtained from SCADA data [8], [9]. The estimation procedure becomes, again, iterative and, therefore, a rapid convergence to an estimation error that is lower than what PMUs alone can provide is crucial to render these hybrid systems useful. The goal of our paper is to provide a criterion to ensure the best of both worlds: greater accuracy and faster convergence for the hybrid system. Before describing our contribution, we briefly review the criteria that have been used thus far to select PMUs placements.

1) Related Works: The primary concern of measurement system design for PSSE is to guarantee the *observability* of the grid so that the state can be solved without ambiguities, which typically depends on the *number of measurements* available. Furthermore, it is also essential that the device *locations* are chosen such that they do not result in the formation of *critical measurements*, whose existence makes the system susceptible to inobservability due to measurements loss.

Therefore, conventional placement designs typically aim at minimizing the number and/or the cost of the sensors under various observability constraints, see, e.g.[10]–[15]. More specifically, the work in [10] and [11] ensure observability by enforcing the algebraic invertibility of the linearized load-flow models or enhancing the numerical condition of the linear model [12]. By treating the grid as a graph [16], the schemes in [13]–[15] guarantee topological observability, corresponding to the requirement that all of the buses have a path connected to at least one device. In general, algebraic observability implies topological observability for linear load-flow models but not vice versa [14]. To suppress or eliminate critical measurements, the work in [17]–[21] propose placements that guarantee system observability even in case of device/branch outages or bad data injections. These methods usually take a divide-and-conquer approach and include multiple stages. Specifically, the first stage determines a measurement set with fixed candidates (or size) by cost minimization and then reduces (or selects) measurements within this set to ensure the topological observability. Numerical techniques such as genetic algorithms [22], [23], simulated-annealing [14], and integer linear programming [24] have also been applied in similar placement problems.

In addition to observability, authors have also targeted improvements in the estimation performance. For example, the work in [25] minimizes a linear cost of individual devices subject to a total error constraint, while [26] uses a two-stage approach that first guarantees topological observability and then refines the placement to improve estimation accuracy. In [27]

Manuscript received March 28, 2013; revised April 07, 2013 and July 24, 2013; accepted August 27, 2013. Date of publication October 17, 2013; date of current version February 14, 2014. This work was supported by the U.S. Department of Energy under the TCIPG Project. Part of this work was presented at the IEEE ICASSP 2013, Vancouver, BC, Canada. Paper no. TPWRS-00360-2013.

X. Li and A. Scaglione are with the Department of Electrical and Computer Engineering, University of California, Davis, CA 95616 USA.

T.-H. Chang is with the Department of Electronic and Computer Engineering, National Taiwan University of Science and Technology, Taipei 10067, Taiwan.

Color versions of one or more of the figures in this paper are available online at http://ieeexplore.ieee.org.

Digital Object Identifier 10.1109/TPWRS.2013.2283079

0885-8950 © 2013 IEEE. Personal use is permitted, but republication/redistribution requires IEEE permission.
See http://www.ieee.org/publications_standards/publications/rights/index.html for more information.

Authorized licensed use limited to: Washington State University. Downloaded on October 11,2022 at 04:27:01 UTC from IEEE Xplore. Restrictions apply.

and [28], instead, PMUs are placed iteratively on buses with the highest error (individual or sum), until a budget is met. A greedy method was proposed in [29] for PMU placement by minimizing the estimation errors of the augmented PSSE using voltage and linearized power injection measurements. A similar problem is solved in [30] via convex relaxation and in [31] by maximizing the mutual information between sensor measurements and state vector.

2) Motivation and Contributions: The PMU placements algorithms in the literature target typically a single specific criterion, observability, or accuracy (see the reviews [32], [33]). It was pointed out recently in [32] that these objectives should be considered jointly, because designs for pure observability often have multiple solutions (e.g., [18]), and they are insufficient to provide accurate estimates. In this paper, we revisit this problem from a unified perspective. Specifically, we jointly consider observability, critical measurements, device outages and failures, estimation performance, together with another important criterion that is oftentimes neglected, which is the convergence of the Gauss–Newton (GN) algorithm typically used in state estimation solvers. Our contribution is: 1) the derivation of the convergence-observability-performance (COP) metric to evaluate the numerical properties, estimation performance, and reliability for a given placement and 2) the formulation and solution of the COP-optimal placement as a semidefinite program (SDP) with integer constraints. We also show that the optimization can be solved through a convex transformation, relaxing the integer constraints. The performance of our design framework is compared successfully with alternatives in simulations.

Notations: We used the following notations.

i	Imaginary unit and $\mathbb{R}$ and $\mathbb{C}$: real and complex numbers.
$\Re\{\cdot\}$ and $\Im\{\cdot\}$	Real and imaginary part of a number.
$\mathbf{I}_N$	$N \times N$ identity matrix.
$\|\mathbf{A}\|$ and $\|\mathbf{A}\|_F$	2-norm[1] and F-norm of a matrix.
$\mathrm{vec}(\mathbf{A})$	Vectorization of a matrix $\mathbf{A}$.
$\mathbf{A}^T$, $\mathrm{Tr}(\mathbf{A})$, $\lambda_{\min}(\mathbf{A})$, $\lambda_{\max}(\mathbf{A})$	Transpose, trace, minimum and maximum eigenvalues of matrix $\mathbf{A}$.
$\otimes$	Kronecker product
$\mathbb{E}[\cdot]$	Expectation.

Given two symmetric matrices $\mathbf{A}$ and $\mathbf{B}$, expressions $\mathbf{A} \succeq \mathbf{B}$ and $\mathbf{A} \succ \mathbf{B}$ represent that the matrix $(\mathbf{A} - \mathbf{B})$ is positive semidefinite and positive definite respectively (i.e., its eigenvalues are all non-negative or positive).

II. Measurement Model and State Estimation

We consider a power grid with N *buses* (i.e., substations), representing interconnections, generators or loads. They are denoted by the set $\mathcal{N} \triangleq \{1, \cdots, N\}$, which form the edge set $\mathcal{E} \triangleq \{\{n, m\}\}$ of cardinality $|\mathcal{E}| = L$, with $\{n, m\}$ denoting the transmission line between n and m. Furthermore, we define $\mathcal{N}(n) \triangleq \{m : \{n, m\} \in \mathcal{E}\}$ as the neighbor of bus n and let $L_n = |\mathcal{N}(n)|$. Control centers collect measurements on certain buses and transmission lines to estimate the state of the power system, i.e., the voltage phasor $V_n \in \mathbb{C}$ at each bus $n \in \mathcal{N}$. In this paper, we consider the Cartesian coordinate representation using the real and imaginary components of the complex voltage phasors $\mathbf{v} = [\Re\{V_1\}, \cdots, \Re\{V_N\}, \Im\{V_1\}, \cdots, \Im\{V_N\}]^T$. This representation facilitates our derivations because it expresses PMU measurements as a linear mapping and SCADA measurements as quadratic forms of the state $\mathbf{v}$ (see [34]).

A. Hybrid State Estimation

The measurement set used in PSSE contains SCADA measurements and PMU measurements from the WAMS. Since there are two complex nodal variables at each bus (i.e., power injection and voltage) and four complex line measurements (i.e., power flow and current), the total number of variables is $2M$, considering real and imaginary parts, where $M = 2N+4L$ is the total number of either the PMU (i.e., voltage and current) or SCADA (i.e., power injection and flow) variables in the ensemble. Thus, the ensemble of variables can be partitioned into four vectors $\mathbf{z} = [\mathbf{z}_{\mathcal{V}}^T, \mathbf{z}_{\mathcal{C}}^T, \mathbf{z}_{\mathcal{I}}^T, \mathbf{z}_{\mathcal{F}}^T]^T$, containing the $2N$ voltage phasor $\mathbf{z}_{\mathcal{V}}$ and power injection vector $\mathbf{z}_{\mathcal{I}}$ at bus $n \in \mathcal{N}$, the $4L$ current phasor $\mathbf{z}_{\mathcal{C}}$, and power flow vector $\mathbf{z}_{\mathcal{F}}$ on line $\{n, m\} \in \mathcal{E}$ at bus n. Note that the subscripts $\mathcal{V}$, $\mathcal{C}$, $\mathcal{I}$, and $\mathcal{F}$ are chosen to indicate "voltage," "current," "injection," and "flow," respectively. The power flow equations $\mathbf{f}_{\mathcal{V}}(\mathbf{v})$, $\mathbf{f}_{\mathcal{C}}(\mathbf{v})$, $\mathbf{f}_{\mathcal{I}}(\mathbf{v})$, and $\mathbf{f}_{\mathcal{F}}(\mathbf{v})$ are specified in Appendix A for different types of measurements. Letting $\mathbf{v}_{\mathrm{true}}$ be the true system state, we have

$$\mathbf{z} = \mathbf{f}(\mathbf{v}_{\mathrm{true}}) + \mathbf{r} \tag{1}$$

where $\mathbf{r} = [\mathbf{r}_{\mathcal{V}}^T, \mathbf{r}_{\mathcal{C}}^T, \mathbf{r}_{\mathcal{I}}^T, \mathbf{r}_{\mathcal{F}}^T]^T$ is the aggregate measurement noise vector, with $\mathbb{E}\{\mathbf{r}\} = \mathbf{0}$ and a covariance matrix $\mathbf{R} \triangleq \mathbb{E}\{\mathbf{r}\mathbf{r}^T\}$, and $\mathbf{f}(\mathbf{v}) = [\mathbf{f}_{\mathcal{V}}^T(\mathbf{v}), \mathbf{f}_{\mathcal{C}}^T(\mathbf{v}), \mathbf{f}_{\mathcal{I}}^T(\mathbf{v}), \mathbf{f}_{\mathcal{F}}^T(\mathbf{v})]^T$ refer to the aggregate power flow equations.

The actual measurements set used in PSSE is a subset of $\mathbf{z}$ in (1), depending on the SCADA and WAMS sensors deployment. Specifically, we introduce a $2M \times 2M$ mask

$$\mathbf{J}_{\mathcal{A}} \triangleq \mathrm{diag}[\mathbf{J}_{\mathcal{V}}, \mathbf{J}_{\mathcal{C}}, \mathbf{J}_{\mathcal{I}}, \mathbf{J}_{\mathcal{F}}] \tag{2}$$

where $\mathbf{J}_{\mathcal{V}}, \mathbf{J}_{\mathcal{C}}, \mathbf{J}_{\mathcal{I}}$, and $\mathbf{J}_{\mathcal{F}}$ are the diagonal masks for each measurement type, having 1 on its diagonal if that measurement is chosen. Applying this mask on the ensemble $\mathbf{z}$ gives

$$\mathbf{J}_{\mathcal{A}}\mathbf{z} = \mathbf{J}_{\mathcal{A}}\mathbf{f}(\mathbf{v}_{\mathrm{true}}) + \mathbf{J}_{\mathcal{A}}\mathbf{r}. \tag{3}$$

The vector $\mathbf{J}_{\mathcal{A}}\mathbf{z}$ are the measurements used in estimation, having non-zero entries selected by $\mathbf{J}_{\mathcal{A}}$ and zero otherwise.

Assuming that the noise is uncorrelated with constant variances for each type, $\mathbf{R} = \mathrm{diag}[\sigma_{\mathcal{V}}^2\mathbf{I}, \sigma_{\mathcal{C}}^2\mathbf{I}, \sigma_{\mathcal{I}}^2\mathbf{I}, \sigma_{\mathcal{F}}^2\mathbf{I}]$. The state is

$$\mathbf{v}_{\mathrm{est}} = \underset{\mathbf{v} \in \mathbb{V}}{\arg\min} \|\mathbf{z}_{\mathcal{A}} - \mathbf{f}_{\mathcal{A}}(\mathbf{v})\|^2 \tag{4}$$

where $\mathbf{z}_{\mathcal{A}} = \mathbf{R}^{-\frac{1}{2}}\mathbf{J}_{\mathcal{A}}\mathbf{z}$ and $\mathbf{f}_{\mathcal{A}}(\mathbf{v}) = \mathbf{R}^{-\frac{1}{2}}\mathbf{J}_{\mathcal{A}}\mathbf{f}(\mathbf{v})$ are the reweighted versions of $\mathbf{z}$ and $\mathbf{f}(\mathbf{v})$ by the covariance $\mathbf{R}$, and

[1]The 2-norm of a matrix is the maximum of the absolute value of the eigenvalues and the 2-norm of a vector $\mathbf{x} \in \mathbb{R}^N$ is $\|\mathbf{x}\| = \sqrt{\sum_{n=1}^N x_n^2}$.

Authorized licensed use limited to: Washington State University. Downloaded on October 11,2022 at 04:27:01 UTC from IEEE Xplore. Restrictions apply.

$\mathbb{V} \triangleq (0, V_{\max}]^{2N}$ is the state space. Without loss of generality, the GN algorithm is usually used to solve (4) for the state.

Although there are variants of the GN algorithm, we study the most basic form of GN updates

$$\mathbf{v}^{k+1} = \mathbf{v}^k + \mathbf{d}^k, \quad k = 1, 2, \cdots \tag{5}$$

with a chosen *initializer* $\mathbf{v}^0$ and the iterative *descent*

$$\mathbf{d}^k = \left[\mathbf{F}_{\mathcal{A}}^T(\mathbf{v}^k)\mathbf{F}_{\mathcal{A}}(\mathbf{v}^k)\right]^{-1}\mathbf{F}_{\mathcal{A}}^T(\mathbf{v}^k)\left[\mathbf{z}_{\mathcal{A}} - \mathbf{f}_{\mathcal{A}}(\mathbf{v}^k)\right] \tag{6}$$

where $\mathbf{F}_{\mathcal{A}}^T(\mathbf{v})\mathbf{F}_{\mathcal{A}}(\mathbf{v})$ is called the *gain matrix* and $\mathbf{F}_{\mathcal{A}}(\mathbf{v}) = \mathbf{R}^{-\frac{1}{2}}\mathbf{J}_{\mathcal{A}}\mathrm{d}\mathbf{f}(\mathbf{v})/\mathrm{d}\mathbf{v}^T$ is the Jacobian corresponding to the selected measurements. The full Jacobian $\mathbf{F}(\mathbf{v}) \triangleq \mathrm{d}\mathbf{f}(\mathbf{v})/\mathrm{d}\mathbf{v}^T$ is computed in Appendix A.

B. Gain Matrix and the PMU Placement

The design of $\mathbf{J}_{\mathcal{A}}$ is crucial for the success of PSSE because $\mathbf{J}_{\mathcal{A}}$ affects the condition number of the gain matrix in (6), which determines the observability of the grid, the stability of the update of state estimates and the ultimate accuracy of the estimates (see the corresponding connections between the gain matrix and these issues in Sections III-A, III-B, and III-C). The goal of this subsection is to express explicitly the dependency of the gain matrix on the PMU placement. Since SCADA systems have been deployed for decades, we assume that SCADA measurements are given so that $\mathbf{J}_{\mathcal{I}}, \mathbf{J}_{\mathcal{F}}$ are fixed and focus on designing the PMU placement $\mathbf{J}_{\mathcal{V}}, \mathbf{J}_{\mathcal{C}}$. We consider the case where each installed PMU captures the voltage and all incident current measurements on that bus as in [14] and [30], so that the current selections $\mathbf{J}_{\mathcal{C}}$ depend entirely on $\mathbf{J}_{\mathcal{V}}$. Therefore, we define the PMU placement vector as

$$\boldsymbol{\mathcal{V}} \triangleq [\mathcal{V}_1, \cdots, \mathcal{V}_N]^T, \quad \mathcal{V}_n \in \{0, 1\} \tag{7}$$

indicating if the nth bus has a PMU and $\mathbf{J}_{\mathcal{V}} = \mathbf{I}_2 \otimes \mathrm{diag}(\boldsymbol{\mathcal{V}})$, while the power injection and power flow measurement placements are given by $\boldsymbol{\mathcal{I}} \triangleq [\mathcal{I}_n]_{N\times 1}$ and $\boldsymbol{\mathcal{F}} \triangleq [\mathcal{F}_{nm}]_{N\times N}$ where $\mathcal{I}_n$ and $\mathcal{F}_{nm} \in \{0, 1\}$ indicate whether the injection at bus n and power flow on line $\{n, m\}$ measured at bus n are present in the PSSE. Similarly, we have $\mathbf{J}_{\mathcal{I}} = \mathbf{I}_2 \otimes \mathrm{diag}(\boldsymbol{\mathcal{I}})$ and $\mathbf{J}_{\mathcal{F}} = \mathbf{I}_2 \otimes \mathrm{diag}[\mathrm{vec}(\boldsymbol{\mathcal{F}})]$. Finally, given an arbitrary state $\mathbf{v}$, the gain matrix in (6) can be decomposed into two components:

$$\mathbf{F}_{\mathcal{A}}^T(\mathbf{v})\mathbf{F}_{\mathcal{A}}(\mathbf{v}) = \mathcal{P}(\boldsymbol{\mathcal{V}}) + \mathcal{S}(\mathbf{v}\mathbf{v}^T, \boldsymbol{\mathcal{I}}, \boldsymbol{\mathcal{F}}) \tag{8}$$

using matrices $\mathbf{H}_{I,n}$, $\mathbf{H}_{J,n}$, $\mathbf{N}_{P,n}$, $\mathbf{N}_{Q,n}$, $\mathbf{E}_{P,nm}$ and $\mathbf{E}_{Q,nm}$ given explicitly by (36) in Appendix A. The exact expression for each component can be analytically written as follows.

1) **PMU data** $\mathcal{P}(\boldsymbol{\mathcal{V}}) : \mathbb{R}^{2N} \to \mathbb{R}^{2N\times 2N}$:

$$\mathcal{P}(\boldsymbol{\mathcal{V}}) = \sum_{n=1}^{N} \mathcal{V}_n \left(\frac{\mathbf{I}_2 \otimes \mathbf{e}_n\mathbf{e}_n^T}{\sigma_{\mathcal{V}}^2} + \frac{\mathbf{H}_{I,n}^T\mathbf{H}_{I,n} + \mathbf{H}_{J,n}^T\mathbf{H}_{J,n}}{\sigma_{\mathcal{C}}^2} \right).$$

2) **SCADA data** $\mathcal{S}(\mathbf{V}, \boldsymbol{\mathcal{I}}, \boldsymbol{\mathcal{F}}) : \mathbb{R}^{2N\times 2N} \to \mathbb{R}^{2N\times 2N}$:

$$\begin{aligned}
&\mathcal{S}(\mathbf{V}, \boldsymbol{\mathcal{I}}, \boldsymbol{\mathcal{F}}) \\
&= \sum_{n=1}^{N} \frac{\mathcal{I}_n}{\sigma_{\mathcal{I}}^2} \left(\mathbf{N}_{P,n} + \mathbf{N}_{P,n}^T\right)^T \mathbf{V} \left(\mathbf{N}_{P,n} + \mathbf{N}_{P,n}^T\right) \\
&+ \sum_{n=1}^{N} \frac{\mathcal{I}_n}{\sigma_{\mathcal{I}}^2} \left(\mathbf{N}_{Q,n} + \mathbf{N}_{Q,n}^T\right)^T \mathbf{V} \left(\mathbf{N}_{Q,n} + \mathbf{N}_{Q,n}^T\right) \\
&+ \sum_{n,m} \frac{\mathcal{F}_{nm}}{\sigma_{\mathcal{F}}^2} \left(\mathbf{E}_{P,nm} + \mathbf{E}_{P,nm}^T\right)^T \mathbf{V} \left(\mathbf{E}_{P,nm} + \mathbf{E}_{P,nm}^T\right) \\
&+ \sum_{n,m} \frac{\mathcal{F}_{nm}}{\sigma_{\mathcal{F}}^2} \left(\mathbf{E}_{Q,nm} + \mathbf{E}_{Q,nm}^T\right)^T \mathbf{V} \left(\mathbf{E}_{Q,nm} + \mathbf{E}_{Q,nm}^T\right)
\end{aligned}$$

where $\mathbf{V} = \mathbf{v}\mathbf{v}^T$.

The derivations are tedious but straightforward from (8) and (36) and thus are omitted due to limited space.

Note that, although the PMU placement design is the focus of this paper, we also consider its complementary benefits on the overall reliability of the PSSE mostly based on SCADA data by showing how PMUs can eliminate critical measurements issues, as explained in Section IV.

III. Measurement Placement Design

Here, we address three important aspects of the placement design as a prequel to the comprehensive metric for PMU placement proposed in Section IV, including observability, convergence, and accuracy, which are all derived with respect to the task of performing state estimation. We call this comprehensive metric the *COP metric*, which is an abbreviation for convergence, observability, and performance. In Section IV, we further derive how the PMU placement $\boldsymbol{\mathcal{V}}$ affects this metric analytically. Later, in Section IV, we optimize the placement using this metric under observability constraints in case of measurement loss or device malfunction.

A. Observability

As mentioned previously, observability analysis is the foundation for all PSSE because it guarantees that the selected measurements are sufficient to solve for the state without ambiguity. There are two concepts associated with this issue, which are the *topological observability* and the *numerical (algebraic) observability*. Topological observability, in essence, studies the measurement system as a graph and determines whether the set of nodes corresponding to the measurement set in PSSE constitute a dominating set of the grid (i.e., each node is a direct neighbor of the nodes that provide the measurement set). Numerical observability, instead, is typically based on the linearized decoupled load flow model [35], and recently the PMU model [10], [13]–[15], [18], [19], [22]–[24], [30], [36], [37], focused on the algebraic invertibility of the PSSE problem. Although the topological observability bears different mathematical interpretations than numerical observability, oftentimes they are both valid measures if the admittance matrix does not suffer from singularity [14], [16].

Authorized licensed use limited to: Washington State University. Downloaded on October 11,2022 at 04:27:01 UTC from IEEE Xplore. Restrictions apply.

Remark 1 (Observability): Using the gain matrix expression in (8), the observability can be guaranteed by having

$$\beta(\boldsymbol{\mathcal{V}}) = \inf_{\mathbf{v}\in\mathbb{V}} \lambda_{\min}\left[\mathcal{P}(\boldsymbol{\mathcal{V}}) + \mathcal{S}(\mathbf{v}\mathbf{v}^T, \boldsymbol{\mathcal{I}}, \boldsymbol{\mathcal{F}})\right] > 0. \tag{9}$$

Given a fixed SCADA placement $\boldsymbol{\mathcal{I}}$ and $\boldsymbol{\mathcal{F}}$, the value of $\beta(\boldsymbol{\mathcal{V}})$ depends on the PMU placement $\boldsymbol{\mathcal{V}}$ which should, therefore, be designed so that $\beta(\boldsymbol{\mathcal{V}}) > 0$. Although observability guarantees the existence and uniqueness of the PSSE solution, it does not imply that the state estimate obtained from the GN algorithm (5) is the correct state estimate, since the solution could be a local minimum. This is especially the case when the initializer $\mathbf{v}^0$ is not chosen properly. Thus, observability is a meaningful criterion only if one assumes successful convergence, as discussed next.

B. Convergence

The convergence of state estimation to the correct estimate $\mathbf{v}_{\rm est}$ using the ac power flow models in (4) has been a critical issue in PSSE. With SCADA measurements, state estimation based on the ac power flow model in (4) is in general nonconvex, and there might be multiple *fixed points* $\mathbf{v}^\star$ of the update in (5) that stop the iterate $\mathbf{v}^k$ from progressing towards the correct estimate $\mathbf{v}_{\rm est}$. Let the set of fixed points $\mathbf{v}^\star$ be

$$\mathbb{V}^\star = \left\{\mathbf{v}\in\mathbb{R}^{2N} : \mathbf{F}_{\mathcal{A}}^T(\mathbf{v})\left[\mathbf{z}_{\mathcal{A}} - \mathbf{f}_{\mathcal{A}}(\mathbf{v})\right] = \mathbf{0}\right\}. \tag{10}$$

Clearly, the correct estimate $\mathbf{v}_{\rm est}$ of (4) is in this set $\mathbf{v}_{\rm est}\in\mathbb{V}^\star$. As a result, there are two convergence issues to address, including a proper *initialization* $\mathbf{v}^0$ and the stabilization of the error $\|\mathbf{v}^k - \mathbf{v}_{\rm est}\|$ made relative the global estimate $\mathbf{v}_{\rm est}\in\mathbb{V}^\star$ instead of other fixed points $\mathbf{v}^\star\in\mathbb{V}^\star$. Because an accurate measurement of the state can be directly obtained by the PMU device, it is natural to exploit such measurements as a good initializer to start the GN algorithm. In the following, we first explain the PMU-assisted initialization scheme, and then present the error dynamics analysis.

We propose to choose the initializer $\mathbf{v}^0$ to match PMU measurements on PMU-instrumented buses, with the rest provided by an arbitrary initializer $\mathbf{v}_{\rm prior}$. The initializer is expressed as

$$\mathbf{v}^0 = \mathbf{J}_{\mathcal{V}}\mathbf{z}_{\mathcal{V}} + (\mathbf{I}_{2N} - \mathbf{J}_{\mathcal{V}})\mathbf{v}_{\rm prior} \tag{11}$$

where $\mathbf{v}_{\rm prior}$ is a stale estimate or nominal profile, and $\mathbf{J}_{\mathcal{V}} = \mathbf{I}_2\otimes{\rm diag}(\boldsymbol{\mathcal{V}})$. Given a placement $\boldsymbol{\mathcal{V}}$, we analyze the error dynamics of the update in (5), which examines the iterative error progression over iterations as a result of the placement.

Lemma 1: Defining the iterative error at the kth update as $\rho_k = \|\mathbf{v}^k - \mathbf{v}_{\rm est}\|$, we have the following error dynamics:

$$\rho_{k+1} \le \frac{1}{2}\sqrt{\frac{\phi_k}{\beta(\boldsymbol{\mathcal{V}})}}\rho_k^2 + \frac{\epsilon\sqrt{2\phi_k}}{\beta(\boldsymbol{\mathcal{V}})}\rho_k. \tag{12}$$

$\epsilon = \|\mathbf{z}_{\mathcal{A}} - \mathbf{f}_{\mathcal{A}}(\mathbf{v}_{\rm est})\|$ is the optimal reconstruction error and

$$\phi_k = \frac{\left(\mathbf{v}^k - \mathbf{v}_{\rm est}\right)^T\mathbf{M}\left(\mathbf{v}^k - \mathbf{v}_{\rm est}\right)}{\left(\mathbf{v}^k - \mathbf{v}_{\rm est}\right)^T\left(\mathbf{v}^k - \mathbf{v}_{\rm est}\right)} \tag{13}$$

is a Rayleigh quotient of the matrix $\mathbf{M}\triangleq\mathcal{S}(\mathbf{I}_{2N}, \boldsymbol{\mathcal{I}}, \boldsymbol{\mathcal{F}})$, equal to $\mathcal{S}(\mathbf{V}, \boldsymbol{\mathcal{I}}, \boldsymbol{\mathcal{F}})$ in (8) with $\mathbf{V} = \mathbf{I}_{2N}$.

Proof: See the results we proved in [38]. ∎

Lemma 1 describes the coupled dynamics of the error ρ_k and the quantity ϕ_k. However, we are only interested in the dynamics of ρ_k, which govern how fast the state estimate reaches the ultimate accuracy. Let us denote an upper bound[2] $\phi(\boldsymbol{\mathcal{V}})$ for all ϕ_k that depends on $\boldsymbol{\mathcal{V}}$. From Lemma 1, Theorem 1 follows.

Theorem 1 [39, Theorem 1]: Given an upper bound $\phi(\boldsymbol{\mathcal{V}}) \ge \phi_k$ for all k and supposing that $\epsilon\sqrt{2\phi(\boldsymbol{\mathcal{V}})} < \beta(\boldsymbol{\mathcal{V}})$, then the algorithm converges $\lim_{k\to\infty}\rho_k = 0$ if the initialization satisfies

$$\rho_0 \le 2\sqrt{\frac{\beta(\boldsymbol{\mathcal{V}})}{\phi(\boldsymbol{\mathcal{V}})}} - \frac{2\sqrt{2}\epsilon}{\sqrt{\beta(\boldsymbol{\mathcal{V}})}}. \tag{14}$$

Remark 2 (Convergence): With a low optimal reconstruction error $\epsilon\approx 0$, the implications of Lemma 1 and Theorem 1 are given here.

- The sensitivity to initialization is determined by the radius

$$\rho_0 \le 2\sqrt{\frac{\beta(\boldsymbol{\mathcal{V}})}{\phi(\boldsymbol{\mathcal{V}})}}. \tag{15}$$

- The error converges quadratically at an asymptotic rate

$$\lim_{k\to\infty}\frac{\rho_{k+1}}{\rho_k^2} \le \frac{1}{2}\sqrt{\frac{\phi(\boldsymbol{\mathcal{V}})}{\beta(\boldsymbol{\mathcal{V}})}}. \tag{16}$$

In other words, the larger the ratio $\beta(\boldsymbol{\mathcal{V}})/\phi(\boldsymbol{\mathcal{V}})$ is, the larger the radius of convergence is and the faster the algorithm converges. Similar to the observability metric in Remark 1, the convergence is determined by the PMU placement $\boldsymbol{\mathcal{V}}$. This is confirmed by simulations in Section V, when $\mathbf{v}^0$ is mildly perturbed. The state estimate diverges drastically to a wrong point if the PMU placement is not chosen carefully and, furthermore, in cases where the algorithm converges, the PMU placement significantly affects the rate of convergence.

What remains to be determined is the bound $\phi(\boldsymbol{\mathcal{V}})$. One simple option is to bound the Rayleigh quotient ϕ_k for each iteration k with the largest eigenvalue $\lambda_{\max}(\mathbf{M})$. However, this is a pessimistic bound that ignores the dependency of ϕ_k on $\mathbf{v}^k$, due to the initialization $\mathbf{v}^0$ in (11). In the proposition below, we motivate the following choice of the upper bound.

Proposition 1: The bound $\phi(\boldsymbol{\mathcal{V}})$ can be approximated by

$$\phi(\boldsymbol{\mathcal{V}}) \approx \lambda_{\max}\left[(\mathbf{I}_{2N} - \mathbf{J}_{\mathcal{V}})^T\mathbf{M}(\mathbf{I}_{2N} - \mathbf{J}_{\mathcal{V}})\right]. \tag{17}$$

Proof: See Appendix B. ∎

C. Performance (Accuracy)

Given Remarks 1 and 2 for observability and convergence, we proceed to discuss the accuracy of the state estimator. This is evaluated by the error between the iterate $\mathbf{v}^k$ and the true state $\mathbf{v}_{\rm true}$, which can be bounded by the triangular inequality

$$\|\mathbf{v}^k - \mathbf{v}_{\rm true}\| \le \|\mathbf{v}^k - \mathbf{v}_{\rm est}\| + \|\mathbf{v}_{\rm est} - \mathbf{v}_{\rm true}\|. \tag{18}$$

[2]Note that the worst case of this upper bound is clearly $\phi(\boldsymbol{\mathcal{V}}) \le \lambda_{\max}(\mathbf{M})$.

Authorized licensed use limited to: Washington State University. Downloaded on October 11,2022 at 04:27:01 UTC from IEEE Xplore. Restrictions apply.

If the iterate $\mathbf{v}^k$ converges stably to the correct estimate $\lim_{k\to\infty}\mathbf{v}^k=\mathbf{v}_{\rm est}$, the error can be bounded accordingly by

$$\lim_{k\to\infty}\|\mathbf{v}^{k+1}-\mathbf{v}_{\rm true}\|\le\|\mathbf{v}_{\rm est}-\mathbf{v}_{\rm true}\|. \tag{19}$$

If the noise $\mathbf{r}$ in (1) is Gaussian, the estimate $\mathbf{v}_{\rm est}$ given by (4) is the maximum likelihood (ML) estimate. According to classic estimation theory [39], the mean square error (MSE) of the ML estimates reaches the Cramér–Rao Bound (CRB) asymptotically given sufficient measurements

$$\mathbb{E}\left[\|\mathbf{v}_{\rm est}-\mathbf{v}_{\rm true}\|^2\right]=\mathrm{Tr}\left[\left(\mathbf{F}_{\mathcal{A}}^T(\mathbf{v}_{\rm true})\mathbf{F}_{\mathcal{A}}(\mathbf{v}_{\rm true})\right)^{-1}\right] \tag{20}$$

where the expectation is with respect to the noise distribution $\mathbf{r}$, and the gain matrix $\mathbf{F}_{\mathcal{A}}^T(\mathbf{v}_{\rm true})\mathbf{F}_{\mathcal{A}}(\mathbf{v}_{\rm true})$ evaluated at the true state $\mathbf{v}_{\rm true}$ is the Fisher Information Matrix (FIM).

Many placement designs focus on lowering the CRB in different ways. Specifically, the A-, M-, and *accuracy* designs[3] in [29], [30] focus on maximizing the trace, the minimum diagonal element, and the minimum eigenvalue of the FIM in (20), respectively. Other existing works considering estimation accuracy optimize their designs with respect to the FIM in an ad-hoc manner. For example, [25] minimizes the cost of PMU deployment under a total error constraint on the trace of the FIM, while [26], [27] are similar to the *M-optimal* design in picking heuristically the locations by pinpointing the maximum entry in the FIM.

Remark 3 (Performance): Given a specific PMU placement $\boldsymbol{\mathcal{V}}$, the MSE of the state estimation is upper bounded as

$$\mathbb{E}\left[\|\mathbf{v}_{\rm est}-\mathbf{v}_{\rm true}\|^2\right]=\mathrm{Tr}\left[\left(\mathbf{F}_{\mathcal{A}}^T(\mathbf{v})\mathbf{F}_{\mathcal{A}}(\mathbf{v})\right)^{-1}\right]\le\frac{2N}{\beta(\boldsymbol{\mathcal{V}}).}$$

Therefore, $\beta(\boldsymbol{\mathcal{V}})$ is an important metric for PMU placements from the observability and performance perspective.

Proof: See the results we proved in [38]. ∎

IV. Optimal PMU Placement via the COP Metric

Based on Remarks 1–3, we are ready to introduce our COP metric

$$\rho(\boldsymbol{\mathcal{V}})=\frac{\beta(\boldsymbol{\mathcal{V}})}{\phi(\boldsymbol{\mathcal{V}})},\quad(\text{COP metric}) \tag{21}$$

where $\beta(\boldsymbol{\mathcal{V}})$ is defined in (9) and $\phi(\boldsymbol{\mathcal{V}})$ is the upper bound (used in Theorem 1) of the Rayleigh quotient ϕ_k in Lemma 1. In fact, it is seen from Remarks 1–3 that the greater the value of $\rho(\boldsymbol{\mathcal{V}})$: 1) the less sensitive PSSE is to initialization; 2) the faster the algorithm converges asymptotically; and 3) the observability and performance metric $\beta(\boldsymbol{\mathcal{V}})$ scales linearly given $\phi(\boldsymbol{\mathcal{V}})$. Therefore, we propose to have the PMUs stabilize the algorithm by giving a good initialization and potentially lowering the estimation error. Next, we exploit the dependency of $\beta(\boldsymbol{\mathcal{V}})$ and $\phi(\boldsymbol{\mathcal{V}})$ on $\boldsymbol{\mathcal{V}}$ to formulate the placement problem.

[3]There is also a *D-optimal* in [29], [30], which minimizes the logarithm of the determinant of the FIM, we omit it because it shares less in common with other related works. In simulations, we compare our design only with the *accuracy* design because of the common objective in maximizing $\beta(\boldsymbol{\mathcal{V}})$. Other A-, D-, and M-*optimal* designs provide similar performances and hence are not repeated in simulations.

We have established the expression of $\beta(\boldsymbol{\mathcal{V}})$ in (8), which however requires an exhaustive search $\mathbf{v}\in\mathbb{V}$. For simplicity, the common practice is to replace the search by substituting the nominal initializer $\mathbf{v}_{\rm prior}$ in (11), where the flat profile is often chosen $\mathbf{v}_{\rm prior}=[\mathbf{1}_N^T,\mathbf{0}_N^T]^T$ as in [30]. This leads to

$$\beta(\boldsymbol{\mathcal{V}})\approx\lambda_{\min}\left[\mathcal{P}(\boldsymbol{\mathcal{V}})+\mathcal{S}(\mathbf{v}_{\rm prior}\mathbf{v}_{\rm prior}^T,\boldsymbol{\mathcal{I}},\boldsymbol{\mathcal{F}})\right]. \tag{22}$$

Thus, given a budget on the number of PMUs $N_{\rm PMU}$ and a total cost constraint $C_{\rm PMU}$, the *optimal* design aims at maximizing the COP metric using the expressions in (22) and (17) to yield

$$\begin{aligned}\max_{\boldsymbol{\mathcal{V}}}\ &\frac{\lambda_{\min}\left[\mathcal{P}(\boldsymbol{\mathcal{V}})+\mathcal{S}(\mathbf{v}_{\rm prior}\mathbf{v}_{\rm prior}^T,\boldsymbol{\mathcal{I}},\boldsymbol{\mathcal{F}})\right]}{\lambda_{\max}\left[(\mathbf{I}_{2N}-\mathbf{J}_{\mathcal{V}})^T\mathbf{M}(\mathbf{I}_{2N}-\mathbf{J}_{\mathcal{V}})\right]}\\ \text{s.t. }&\mathbf{J}_{\mathcal{V}}=\mathbf{I}_2\otimes\mathrm{diag}(\boldsymbol{\mathcal{V}}),\mathcal{V}_n\in\{0,1\}\\ &\mathbf{1}_N^T\boldsymbol{\mathcal{V}}\le N_{\rm PMU},\boldsymbol{c}^T\boldsymbol{\mathcal{V}}\le C_{\rm PMU}\end{aligned} \tag{23}$$

where $\boldsymbol{c}=[c_1,\cdots,c_N]^T$ contains the cost of each PMU.

Note that maximizing the COP metric alone does not necessarily maximize the observability and performance metric $\beta(\boldsymbol{\mathcal{V}})$, but instead it is providing a sweet spot between having a good initialization and lowering the estimation error. To ensure that the value of $\beta(\boldsymbol{\mathcal{V}})$ is sufficiently large, we further consider eliminating critical measurements with a tolerance parameter set by the designer $\beta_{\min}>0$ such that $\beta(\boldsymbol{\mathcal{V}})$ is guaranteed to surpass an acceptable threshold. Another benefit of eliminating critical measurements is to improve bad data detection capability. Therefore, in Section IV-A, we formulate the PMU placement problem by considering reliability constraints on data redundancy and *critical measurements*.

A. Elimination of Critical Measurements

Let us denote by $\boldsymbol{\mathcal{J}}_n$ and $\boldsymbol{\mathcal{G}}_{nm}$ the failure patterns for power injection and flow measurements, where the nth bus injection or the line flow on $\{n,m\}$ measured at bus n is removed from the existing SCADA measurements $\boldsymbol{\mathcal{I}}$ and $\boldsymbol{\mathcal{F}}$. Then, given a tolerance parameter $\beta_{\min}>0$ to ensure the numerical observability,[4] the PMU placement optimization is

$$\begin{aligned}\max_{\boldsymbol{\mathcal{V}}}&\frac{\lambda_{\min}\left[\mathcal{P}(\boldsymbol{\mathcal{V}})+\mathcal{S}(\mathbf{v}_{\rm prior}\mathbf{v}_{\rm prior}^T,\boldsymbol{\mathcal{I}},\boldsymbol{\mathcal{F}})\right]}{\lambda_{\max}\left[(\mathbf{I}_{2N}-\mathbf{J}_{\mathcal{V}})^T\mathbf{M}(\mathbf{I}_{2N}-\mathbf{J}_{\mathcal{V}})\right]},\\ \text{s.t.}&\lambda_{\min}\left[\mathcal{P}(\boldsymbol{\mathcal{V}})+\mathcal{S}(\mathbf{v}_{\rm prior}\mathbf{v}_{\rm prior}^T,\boldsymbol{\mathcal{J}}_n,\boldsymbol{\mathcal{F}})\right]\ge\beta_{\min},\forall n\in\mathcal{N}\\ &\lambda_{\min}\left[\mathcal{P}(\boldsymbol{\mathcal{V}})+\mathcal{S}(\mathbf{v}_{\rm prior}\mathbf{v}_{\rm prior}^T,\boldsymbol{\mathcal{I}},\boldsymbol{\mathcal{G}}_{nm})\right]\ge\beta_{\min},\forall\{n,m\}\in\mathcal{E}\\ &\mathbf{J}_{\mathcal{V}}=\mathbf{I}_2\otimes\mathrm{diag}(\boldsymbol{\mathcal{V}}),\mathcal{V}_n\in\{0,1\}\\ &\mathbf{1}_N^T\boldsymbol{\mathcal{V}}\le N_{\rm PMU},\boldsymbol{c}^T\boldsymbol{\mathcal{V}}\le C_{\rm PMU}.\end{aligned} \tag{24}$$

Remark 4: The constraints above can be easily extended to cover multiple failures by incorporating corresponding outage scenarios $\boldsymbol{\mathcal{J}}_n$ and $\boldsymbol{\mathcal{G}}_{nm}$, which will be necessary in eliminating critical measurement set (i.e., minimally dependent set). Furthermore, topological observability constraints can also be easily added because of their linearity with respect to the placement vector $\boldsymbol{\mathcal{V}}$ as in [13]–[15], [18], and [19]. We omit the full formulation due to lack of space.

[4]The value of $\beta_{\min}$ is set to be 0.01 in simulations for all cases.

Authorized licensed use limited to: Washington State University. Downloaded on October 11,2022 at 04:27:01 UTC from IEEE Xplore. Restrictions apply.

B. Semi-Definite Programming and Relaxation

The eigenvalue problem in (24) can be reformulated via linear matrix inequalities using two dummy variables ϕ and β as

$$\begin{aligned}
&\max_{\boldsymbol{\mathcal{V}},\beta,\phi} \ \frac{\beta}{\phi},\\
&\text{s.t.} \quad \mathcal{P}(\boldsymbol{\mathcal{V}})+\mathcal{S}(\mathbf{v}_{\text{prior}}\mathbf{v}_{\text{prior}}^T,\boldsymbol{\mathcal{I}},\boldsymbol{\mathcal{F}}) \succeq \beta\mathbf{I}\\
&\begin{bmatrix} \phi\mathbf{I}_{2N} & \mathbf{M}^{\frac{1}{2}}(\mathbf{I}_{2N}-\mathbf{J}_{\mathcal{V}}) \\ (\mathbf{I}_{2N}-\mathbf{J}_{\mathcal{V}})^T\mathbf{M}^{\frac{T}{2}} & \mathbf{I}_{2N} \end{bmatrix} \succeq \mathbf{0}\\
&\mathcal{P}(\boldsymbol{\mathcal{V}}) + \mathcal{S}(\mathbf{v}_{\text{prior}}\mathbf{v}_{\text{prior}}^T,\boldsymbol{\mathcal{J}}_n,\boldsymbol{\mathcal{F}}) \succeq \beta_{\min}\mathbf{I}_{2N}, \forall n \in \mathcal{N}\\
&\mathcal{P}(\boldsymbol{\mathcal{V}}) + \mathcal{S}(\mathbf{v}_{\text{prior}}\mathbf{v}_{\text{prior}}^T,\boldsymbol{\mathcal{I}},\boldsymbol{\mathcal{G}}_{nm}) \succeq \beta_{\min}\mathbf{I}_{2N}, \forall \{n,m\} \in \mathcal{E}\\
&\mathbf{J}_{\mathcal{V}} = \mathbf{I}_2 \otimes \text{diag}(\boldsymbol{\mathcal{V}}), \mathcal{V}_n \in \{0,1\}\\
&\mathbf{1}_N^T\boldsymbol{\mathcal{V}} \le N_{\text{PMU}}, \boldsymbol{c}^T\boldsymbol{\mathcal{V}} \le C_{\text{PMU}}.
\end{aligned} \tag{25}$$

To avoid solving this complicated eigenvalue problem with integer constraints, we relax (25) by converting the integer constraint $\mathcal{V}_n \in \{0,1\}$ to a convex constraint $0 \le \mathcal{V}_n \le 1$. Then, the optimization becomes a quasi-convex problem that needs to be solved in an iterative fashion via the classical bisection method by performing a sequence of SDP feasibility problems [40]. Clearly, this consumes considerable computations and is less desirable. Fortunately, since the objective (25) is a linear fractional function, the *Charnes-Cooper* transformation [41] can be used to reformulate the problem in (25) as a single convex SDP, whose global optimum can be obtained in one pass.

Proposition 2: By letting $\gamma = 1/\phi$, $\tau = \beta/\phi$ and $\boldsymbol{\xi} = \boldsymbol{\mathcal{V}}/\phi$, the global optimum solution to (25) without the integer constraint can be determined by

$$\begin{aligned}
&\max_{\boldsymbol{\xi},\tau,\gamma} \ \tau, \quad \text{s.t. } \mathcal{P}(\boldsymbol{\xi}) + \gamma\mathcal{S}(\mathbf{v}_{\text{prior}}\mathbf{v}_{\text{prior}}^T,\boldsymbol{\mathcal{I}},\boldsymbol{\mathcal{F}}) \succeq \tau\mathbf{I}\\
&\qquad\qquad \begin{bmatrix} \mathbf{I} & \mathbf{M}^{\frac{1}{2}}(\gamma\mathbf{I}-\mathbf{I}_{\boldsymbol{\xi}}) \\ (\gamma\mathbf{I}-\mathbf{I}_{\boldsymbol{\xi}})^T\mathbf{M}^{\frac{T}{2}} & \gamma\mathbf{I} \end{bmatrix} \succeq \mathbf{0}\\
&\qquad\qquad \mathcal{P}(\boldsymbol{\xi}) + \gamma\mathcal{S}(\mathbf{v}_{\text{prior}}\mathbf{v}_{\text{prior}}^T,\boldsymbol{\mathcal{J}}_n,\boldsymbol{\mathcal{F}}) \succ \mathbf{0}, \forall n\\
&\qquad\qquad \mathcal{P}(\boldsymbol{\xi})+\gamma\mathcal{S}(\mathbf{v}_{\text{prior}}\mathbf{v}_{\text{prior}}^T,\boldsymbol{\mathcal{I}},\boldsymbol{\mathcal{G}}_{nm}) \succ \mathbf{0}, \forall \{n,m\}\\
&\qquad\qquad \mathbf{I}_{\boldsymbol{\xi}} = \mathbf{I}_2 \otimes \text{diag}(\boldsymbol{\xi}), \xi_n \in [0,\gamma]\\
&\qquad\qquad \mathbf{1}_N^T\boldsymbol{\xi} \le \gamma N_{\text{PMU}}, \boldsymbol{c}^T\boldsymbol{\xi} \le \gamma C_{\text{PMU}}
\end{aligned} \tag{26}$$

whose solution is mapped to the solution of (25) as

$$\boldsymbol{\mathcal{V}}^\star = \frac{\boldsymbol{\xi}^\star}{\gamma^\star}. \tag{27}$$

The solution $\boldsymbol{\mathcal{V}}^\star$ has real values but not the original binary values. Here we use a randomization technique [42] to choose the solution by drawing a group of $\ell_\star$ binary vectors $\boldsymbol{\mathcal{V}}_\ell$ from a Bernoulli distribution on each entry with probabilities obtained from the solution $\boldsymbol{\mathcal{V}}^\star$. Then, we compare the COP metric evaluated at the group of candidates $\{\boldsymbol{\mathcal{V}}_\ell\}_{\ell=1}^{\ell_\star}$ and choose the one that has the maximum as the optimal placement vector. This scheme approximates closely to the optimal solution of the original integer problem as shown in simulations.

V. Simulations

Here, we compare our *proposed* design in different systems mainly against the *accuracy* placement that optimizes estimation accuracy (i.e., *E-optimal* in [29], [30]) and an *observability* placement that satisfies system observability [14] jointly with SCADA measurements. The measurements are generated with independent errors $\mathbf{R} = \sigma^2\mathbf{I}$ and $\sigma^2 = 10^{-4}$. We demonstrate the optimality of our formulation in the IEEE-14 system, and extend the comparison on the convergence and estimation performance for IEEE 30-bus and 118-bus systems, using 15% of all SCADA measurements provided at random.[5]

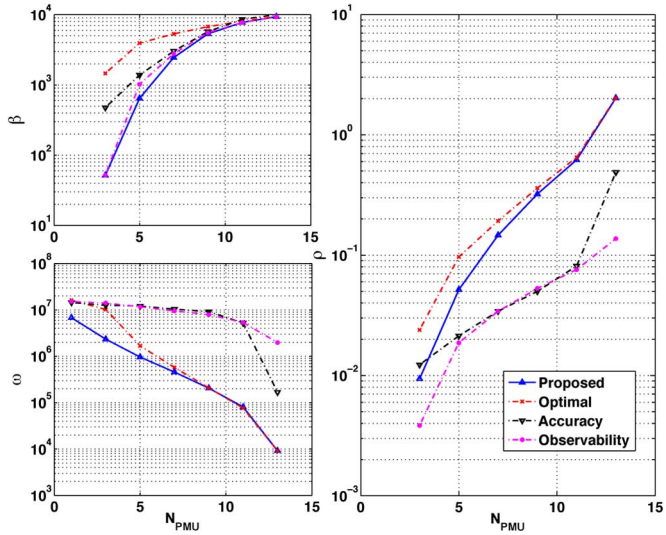

Fig. 1. Comparison of ρ, ϕ and β for the IEEE 14-bus system.

A. IEEE 14-Bus System (Figs. 1 and 2)

We show the optimality of the *proposed* placement in Fig. 1 by comparing ρ, β and ϕ against the *accuracy*, the *observability*, and, most importantly, the exact *optimal* PMU placement in the IEEE 14-bus system for $N_{\text{PMU}} = 1, \cdots, 13$, where the exact *optimal* solution is obtained by an exhaustive search in the nonrelaxed problem (24). It is seen from β that, under 15% SCADA measurements, the system remains unobservable until $N_{\text{PMU}} = 3$ since $\beta = 0$ is not shown on the curve.

A significant gap can be seen in Fig. 1 between the *proposed*, the *optimal*, and the *accuracy* schemes. It is clear that the *proposed* scheme gives a uniformly greater ρ than the *accuracy* scheme and closely touches the *optimal* solution. Clearly, the *accuracy* design achieves a larger β than the *proposed* scheme, but this quantity is less sensitive to the PMU placement than ϕ for all N_{PMU}. This implies that the estimation accuracy of the hybrid state estimation is not very sensitive to the placement, because of the presence of SCADA measurements. In fact, convergence is a more critical issue. In particular, when the PMU budget is low (i.e. N_{PMU} is small), the *accuracy* does not provide discernible improvement on ϕ (thus ρ) while the *optimal* and *proposed* schemes considerably lower ϕ and increase ρ, which stabilizes and accelerates the algorithm convergence without affecting greatly accuracy.

In Fig. 2, we show an example of the *proposed* placement with $N_{\text{PMU}} = 6$ in one experiment where there are 19 SCADA measurements (15% of total) marked in "blue" while there are PMU measurements marked in "red." It can be seen that the

[5]The number of SCADA measurements in each experiment is $15\% \times (4N + 8L)$, where N is the number of buses and L is the number of lines.

Authorized licensed use limited to: Washington State University. Downloaded on October 11,2022 at 04:27:01 UTC from IEEE Xplore. Restrictions apply.

	Power Flow	Power Injection	PMU
Real	(1,5) (4,7) (6,12) (1,2) (2,3) (12,13)	3, 6, 9	1, 2, 4, 5, 6, 8
Imaginary	(4,5) (10,11) (13,14) (4,5) (4,9) (6,11) (9,14)	3, 5, 13	

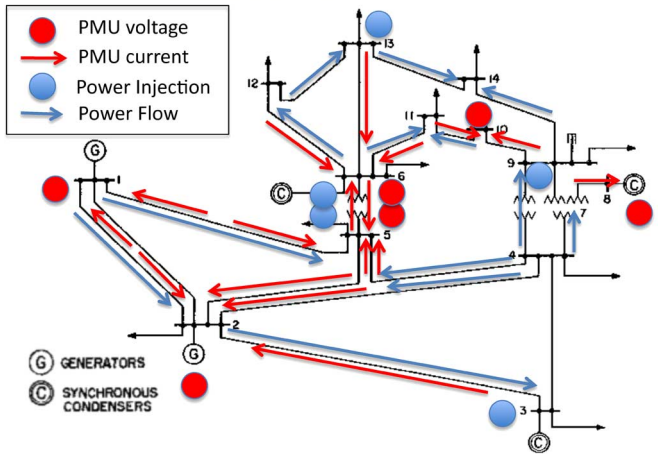

Fig. 2. Example of the proposed placement for the IEEE 14-bus system.

system is always observable even with single failure because each node is metered by the measurements at least twice so there is sufficient redundancy to avoid critical measurements.

B. IEEE 30-Bus and 118-Bus Systems

We illustrate the estimation convergence and performance of our *proposed* placement against the alternatives above and the case with no PMUs, in terms of the total vector error (TVE) in [43] for evaluating the accuracy of PMU-related state estimates

$$\mathrm{TVE}_k = \|\mathbf{v}^k - \mathbf{v}_{\mathrm{true}}\|/\|\mathbf{v}_{\mathrm{true}}\| \times 100\% \qquad (28)$$

for each iteration k. This shows the decrease of TVE as the Gauss–Newton proceeds iteratively, which is a typical way to illustrate convergence behavior and the asymptotic accuracy upon convergence. With 17% PMU deployment, we compare the TVE curves for the IEEE 30-bus system with $N_{\mathrm{PMU}} = 5$ in Fig. 3(a) and the IEEE 118-bus system with $N_{\mathrm{PMU}} = 20$ in Fig. 3(b). To verify the robustness to initialization (numerical stability) and the convergence rate, the TVE curves are averaged over 200 experiments. For each experiment, we generate a placement guaranteeing observability for the *observability* placement according to [14] and use a noninformative initializer $\mathbf{v}_{\mathrm{prior}} = [\mathbf{1}_N^T + 0.1\boldsymbol{\varepsilon}^T, \mathbf{0}_N^T]^T$ perturbed by a zero-mean Gaussian error vector $\boldsymbol{\varepsilon}$ with $\mathbb{E}[\boldsymbol{\varepsilon}\boldsymbol{\varepsilon}^T] = \mathbf{I}$. We leave the imaginary part unperturbed because phases are usually small.

It is seen in Fig. 3(a) that, if there are no PMU installed, it is possible that the algorithm does not converge while the *proposed* placement scheme converges stably. The performance of the *observability* placement is not stably guaranteed even if it satisfies observability because it diverges under perturbations for the 118-bus system in Fig. 3(a). A similar divergent trend can be observed if the initialization is very inaccurate, regardless of how it is set. Consistent with Theorem 1, since the noise σ^2 is small, the algorithm converges quadratically for the *proposed* and the *accuracy* placement, but the convergence rates vary greatly. Although the asymptotic TVE remains comparable, the *proposed* placement considerably accelerates the convergence compared with the *observability* and *accuracy* placement.

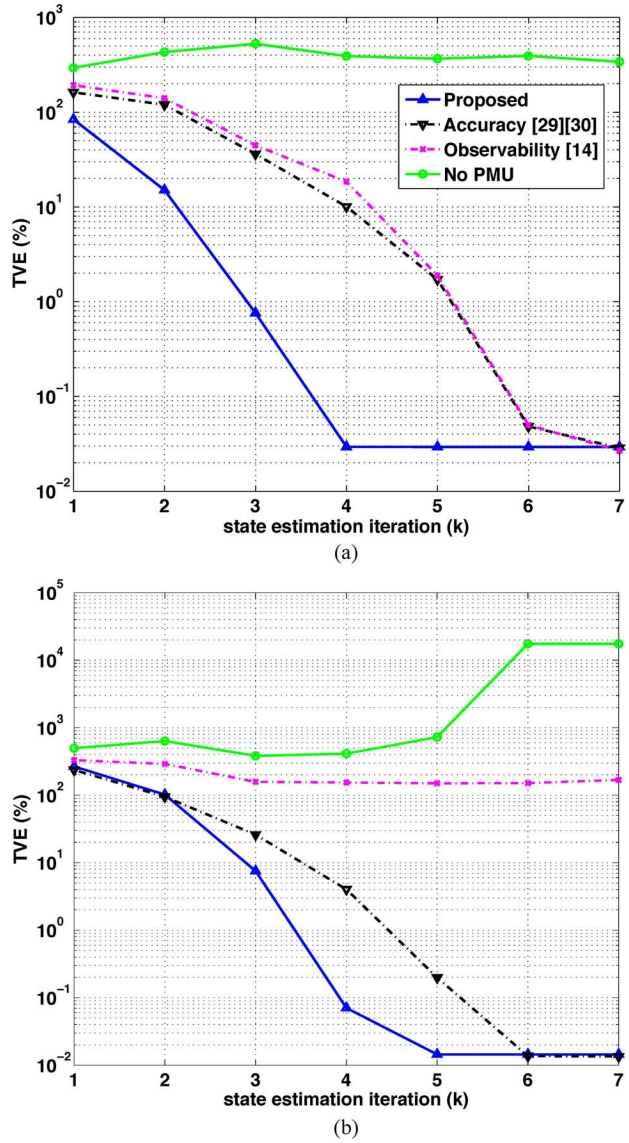

Fig. 3. TVE curves for the IEEE (a) 30-bus and (b) 118-bus systems.

VI. Conclusion

In this paper, we propose a useful metric, referred to as COP, to evaluate the convergence and accuracy of hybrid PSSE for a given sensor deployment, where PMUs are used to initialize the Gauss–Newton iterative estimation. The COP metric is derived from the convergence analysis of the Gauss–Newton state estimation procedures, which is a joint measure for convergence $\phi(\boldsymbol{\mathcal{V}})$ and the FIM as a measure for accuracy and observability $\beta(\boldsymbol{\mathcal{V}})$. We optimize our placement strategy by maximizing the COP metric $\beta(\boldsymbol{\mathcal{V}})/\phi(\boldsymbol{\mathcal{V}})$ via a simple SDP, and the critical measurement constraints in the SDP formulation further ensure that the numerical observability $\beta(\boldsymbol{\mathcal{V}})$ is bounded away from zero up to a tolerable point. Finally, the simulations confirm numerically the convergence and estimation performance of the proposed scheme.

Authorized licensed use limited to: Washington State University. Downloaded on October 11,2022 at 04:27:01 UTC from IEEE Xplore. Restrictions apply.

APPENDIX

A. Power Flow Equations and Jacobian Matrix

The admittance matrix $\mathbf{Y} = [-Y_{nm}]_{N\times N}$, includes line admittances $Y_{nm} = G_{nm} + \mathrm{i}B_{nm}$, $\{n,m\} \in \mathcal{E}$ and bus admittance-to-ground $\bar{Y}_{nm} = \bar{G}_{nm} + \mathrm{i}\bar{B}_{nm}$ in the Π-model of line $\{n,m\} \in \mathcal{E}$, and self-admittance $Y_{nn} = -\sum_{m\neq n}(\bar{Y}_{nm} + Y_{nm})$. Using the canonical basis $\mathbf{e}_n = [0,\cdots,1,\cdots,0]^T$ and the matrix $\mathbf{Y}$, we define the following matrices:

$$\mathbf{Y}_n \triangleq \mathbf{e}_n\mathbf{e}_n^T\mathbf{Y}, \quad \mathbf{Y}_{nm} \triangleq (Y_{nm}+\bar{Y}_{nm})\mathbf{e}_n\mathbf{e}_n^T - Y_{nm}\mathbf{e}_n\mathbf{e}_m^T.$$

Letting $\mathbf{G}_n = \Re\{\mathbf{Y}_n\}$, $\mathbf{B}_n = \Im\{\mathbf{Y}_n\}$, $\mathbf{G}_{nm} = \Re\{\mathbf{Y}_{nm}\}$, and $\mathbf{B}_{nm} = \Im\{\mathbf{Y}_{nm}\}$, we define the following matrices:

$$\mathbf{N}_{P,n} \triangleq \begin{bmatrix} \mathbf{G}_n & -\mathbf{B}_n \\ \mathbf{B}_n & \mathbf{G}_n \end{bmatrix} \qquad \mathbf{N}_{Q,n} \triangleq -\begin{bmatrix} \mathbf{B}_n & \mathbf{G}_n \\ -\mathbf{G}_n & \mathbf{B}_n \end{bmatrix}$$
$$\mathbf{E}_{P,nm} \triangleq \begin{bmatrix} \mathbf{G}_{nm} & -\mathbf{B}_{nm} \\ \mathbf{B}_{nm} & \mathbf{G}_{nm} \end{bmatrix} \quad \mathbf{E}_{Q,nm} \triangleq -\begin{bmatrix} \mathbf{B}_{nm} & \mathbf{G}_{nm} \\ -\mathbf{G}_{nm} & \mathbf{B}_{nm} \end{bmatrix}$$
$$\mathbf{C}_{I,nm} \triangleq \begin{bmatrix} \mathbf{G}_{nm} & \mathbf{0} \\ \mathbf{0} & -\mathbf{B}_{nm} \end{bmatrix} \quad \mathbf{C}_{J,nm} \triangleq \begin{bmatrix} \mathbf{B}_{nm} & \mathbf{0} \\ \mathbf{0} & \mathbf{G}_{nm} \end{bmatrix}.$$

The SCADA system collects active/reactive injection (P_n, Q_n) at bus n and flow (P_{nm}, Q_{nm}) at bus n on line $\{n,m\}$ to yield

$$P_n = \mathbf{v}^T\mathbf{N}_{P,n}\mathbf{v}, \quad Q_n = \mathbf{v}^T\mathbf{N}_{Q,n}\mathbf{v}, \tag{29}$$
$$P_{nm} = \mathbf{v}^T\mathbf{E}_{P,nm}\mathbf{v}, \quad Q_{nm} = \mathbf{v}^T\mathbf{E}_{Q,nm}\mathbf{v} \tag{30}$$

and stacks them in the power flow equations

$$\mathbf{f}_{\mathcal{I}}(\mathbf{v}) = [\cdots, P_n, \cdots, \cdots, Q_n, \cdots]^T \tag{31}$$
$$\mathbf{f}_{\mathcal{F}}(\mathbf{v}) = [\cdots, P_{nm}, \cdots, \cdots, Q_{nm}, \cdots]^T. \tag{32}$$

The WAMS collects the voltage $(\Re\{V_n\}, \Im\{V_n\})$ at bus n and the current (I_{nm}, J_{nm}) on line $\{n,m\}$ measured at bus n as

$$I_{nm} = (\mathbf{1}_2 \otimes \mathbf{e}_n)^T\mathbf{C}_{I,nm}\mathbf{v} \tag{33}$$
$$J_{nm} = (\mathbf{1}_2 \otimes \mathbf{e}_n)^T\mathbf{C}_{J,nm}\mathbf{v} \tag{34}$$

where $\otimes$ is the Kronecker product and stacks them as

$$\mathbf{f}_{\mathcal{V}}(\mathbf{v}) = \mathbf{v}, \mathbf{f}_{\mathcal{C}}(\mathbf{v}) = [\cdots, I_{nm}, \cdots, \cdots, J_{nm}, \cdots]^T. \tag{35}$$

The Jacobian $\mathbf{F}(\mathbf{v})$ can be derived from (33), (29), and (30) to yield

$$\mathbf{F}^T(\mathbf{v}) = \left[\mathbf{I}_{2N}, \mathbf{H}_{\mathcal{C}}^T, \mathbf{H}_{\mathcal{I}}^T(\mathbf{I}_{2N}\otimes\mathbf{v}), \mathbf{H}_{\mathcal{F}}^T(\mathbf{I}_{4L}\otimes\mathbf{v})\right] \tag{36}$$

where

$$\mathbf{H}_{\mathcal{C}} \triangleq \left[\cdots, \mathbf{H}_{I,n}^T, \cdots, \cdots, \mathbf{H}_{J,n}^T, \cdots\right]^T$$
$$\mathbf{H}_{\mathcal{I}} \triangleq \left[\cdots, \mathbf{N}_{P,n} + \mathbf{N}_{P,n}^T, \cdots, \mathbf{N}_{Q,n} + \mathbf{N}_{Q,n}^T, \cdots\right]^T$$
$$\mathbf{H}_{\mathcal{F}} \triangleq \left[\cdots, \mathbf{E}_{P,nm} + \mathbf{E}_{P,nm}^T, \cdots, \mathbf{E}_{Q,nm} + \mathbf{E}_{Q,nm}^T, \cdots\right]^T$$

using $\mathbf{S}_n \triangleq \mathbf{I}_{L_n} \otimes (\mathbf{1}_2 \otimes \mathbf{e}_n)^T$ and

$$\mathbf{H}_{I,n} \triangleq \mathbf{S}_n\mathbf{C}_{I,n}, \quad \mathbf{C}_{I,n} \triangleq \left[\cdots, \mathbf{C}_{I,nm}^T, \cdots\right]^T$$
$$\mathbf{H}_{J,n} \triangleq \mathbf{S}_n\mathbf{C}_{J,n}, \quad \mathbf{C}_{J,n} \triangleq \left[\cdots, \mathbf{C}_{J,nm}^T, \cdots\right]^T. \tag{37}$$

B. Proof of Proposition 1

To maintain tractability, the $\phi(\boldsymbol{\mathcal{V}})$ in the COP metric is approximated by the first Rayleigh quotient ϕ_0 resulting from initialization. Therefore, we upper bound ϕ_0 assuming that the noise in the PMU is negligible,[6] then $\mathbf{z}_{\mathcal{V}} = \mathbf{v}_{\text{true}} \approx \mathbf{v}_{\text{est}}$ and therefore $\mathbf{v}^0 - \mathbf{v}_{\text{est}} \approx (\mathbf{I}_{2N} - \mathbf{J}_{\mathcal{V}})(\mathbf{v}_{\text{prior}} - \mathbf{v}_{\text{est}})$, implying that

$$\phi_0 \approx \frac{(\mathbf{v}_{\text{prior}}-\mathbf{v}_{\text{est}})^T(\mathbf{I}_{2N}-\mathbf{J}_{\mathcal{V}})^T\mathbf{M}(\mathbf{I}_{2N}-\mathbf{J}_{\mathcal{V}})(\mathbf{v}_{\text{prior}}-\mathbf{v}_{\text{est}})}{(\mathbf{v}_{\text{prior}}-\mathbf{v}_{\text{est}})^T(\mathbf{I}_{2N}-\mathbf{J}_{\mathcal{V}})^T(\mathbf{I}_{2N}-\mathbf{J}_{\mathcal{V}})(\mathbf{v}_{\text{prior}}-\mathbf{v}_{\text{est}})}.$$

Considering the impotence of $(\mathbf{I}_{2N} - \mathbf{J}_{\mathcal{V}}) = (\mathbf{I}_{2N} - \mathbf{J}_{\mathcal{V}})^2$ in the numerator, the approximate bound is obtained as (17).

REFERENCES

[1] X. Li, A. Scaglione, and T.-H. Chang, "Optimal sensor placement for hybrid state estimation in smart grid," in *Proc. IEEE Int. Conf. Acoust., Speech Signal Process.*, Vancouver, BC, Canada.

[2] J. Chow, P. Quinn, L. Beard, D. Sobajic, A. Silverstein, and L. Vanfretti, "Guidelines for siting phasor measurement units: Version 8, June, 15 2011," North American SynchroPhasor Initiative (NASPI) Res. Initiative Task Team, 2011.

[3] T. Yang, H. Sun, and A. Bose, "Transition to a two-level linear state estimator: Part I & II," *IEEE Trans. Power Syst.*, no. 26, pp. 46–53, 2011.

[4] A. Phadke, J. Thorp, and K. Karimi, "State estimation with phasor measurements," *IEEE Power Eng. Rev.*, no. 2, pp. 48–48, 1986.

[5] A. Meliopoulos, G. Cokkinides, C. Hedrington, and T. Conrad, "The supercalibrator—a fully distributed state estimator," in *Proc. IEEE Power and Energy Soc. General Meeting*, 2010, pp. 1–8.

[6] X. Qin, T. Bi, and Q. Yang, "Hybrid non-linear state estimation with voltage phasor measurements," in *Proc. IEEE Power Eng. Soc. General Meeting*, 2007, pp. 1–6.

[7] R. Nuqui and A. Phadke, "Hybrid linear state estimation utilizing synchronized phasor measurements," in *Proc. IEEE Power Tech*, Lausanne, Switzerland, 2007, pp. 1665–1669, IEEE.

[8] S. Chakrabarti, E. Kyriakides, G. Ledwich, and A. Ghosh, "A comparative study of the methods of inclusion of PMU current phasor measurements in a hybrid state estimator," in *Proc. IEEE Power and Energy Soc. Gen. Meeting*, 2010, pp. 1–7.

[9] R. Avila-Rosales, M. Rice, J. Giri, L. Beard, and F. Galvan, "Recent experience with a hybrid SCADA/PMU online state estimator," in *Proc. IEEE Power & Energy Soc. Gen. Meeting*, 2009, pp. 1–8.

[10] B. Gou, "Optimal placement of PMUs by integer linear programming," *IEEE Trans. Power Syst.*, vol. 23, no. 3, pp. 1525–1526, Aug. 2008.

[11] B. Gou and A. Abur, "An improved measurement placement algorithm for network observability," *IEEE Trans. Power Syst.*, vol. 16, no. 4, pp. 819–824, Nov. 2001.

[12] C. Madtharad, S. Premrudeepreechacharn, N. Watson, and D. Saenrak, "Measurement placement method for power system state estimation: Part I," in *Proc. IEEE Power Eng. Soc. Gen. Meeting*, Jul. 13-17, 2003, vol. 3, p. 1632.

[13] R. Emami and A. Abur, "Robust measurement design by placing synchronized phasor measurements on network branches," *IEEE Trans. Power Syst.*, vol. 25, no. 1, pp. 38–43, Feb. 2010.

[14] T. Baldwin, L. Mili, M. Boisen, Jr, and R. Adapa, "Power system observability with minimal phasor measurement placement," *IEEE Trans. Power Syst.*, vol. 8, no. 2, pp. 707–715, May 1993.

[15] X. Bei, Y. Yoon, and A. Abur, "Optimal placement and utilization of phasor measurements for state estimation," *PSERC Pub. 05–20*, 2005.

[16] K. Clements, "Observability methods and optimal meter placement," *Int. J. Electr. Power Energy Syst.*, vol. 12, no. 2, pp. 88–93, 1990.

[17] F. Magnago and A. Abur, "A unified approach to robust meter placement against loss of measurements and branch outages," *IEEE Trans. Power Syst.*, vol. 15, no. 3, pp. 945–949, Aug. 2000.

[18] S. Chakrabarti and E. Kyriakides, "Optimal placement of phasor measurement units for power system observability," *IEEE Trans. Power Syst.*, vol. 23, no. 3, pp. 1433–1440, Aug. 2008.

[6] If the noise is not sufficiently small to be neglected, the metric becomes random and needs to be optimized on an average whose expression cannot be obtained in closed form. Thus, we consider the small noise case and neglect it.

Authorized licensed use limited to: Washington State University. Downloaded on October 11,2022 at 04:27:01 UTC from IEEE Xplore. Restrictions apply.

[19] S. Chakrabarti, E. Kyriakides, and D. Eliades, "Placement of synchronized measurements for power system observability," *IEEE Trans. Power Del.*, vol. 24, no. 1, pp. 12–19, Jan. 2009.
[20] M. Yehia, R. Jabr, R. El-Bitar, and R. Waked, "A PC based state estimator interfaced with a remote terminal unit placement algorithm," *IEEE Trans. Power Syst.*, vol. 16, no. 2, pp. 210–215, May 2001.
[21] M. Baran, J. Zhu, H. Zhu, and K. Garren, "A meter placement method for state estimation," *IEEE Trans. Power Syst.*, vol. 10, no. 3, pp. 1704–1710, Aug. 1995.
[22] B. Milosevic and M. Begovic, "Nondominated sorting genetic algorithm for optimal phasor measurement placement," *IEEE Trans. Power Syst.*, vol. 18, no. 1, pp. 69–75, Feb. 2003.
[23] F. Aminifar, C. Lucas, A. Khodaei, and M. Fotuhi-Firuzabad, "Optimal placement of phasor measurement units using immunity genetic algorithm," *IEEE Trans. Power Del.*, vol. 24, no. 3, pp. 1014–1020, Jul. 2009.
[24] D. Dua, S. Dambhare, R. Gajbhiye, and S. Soman, "Optimal multistage scheduling of PMU placement: An ILP approach," *IEEE Trans. Power Del.*, vol. 23, no. 4, pp. 1812–1820, Oct. 2008.
[25] Y. Park, Y. Moon, J. Choo, and T. Kwon, "Design of reliable measurement system for state estimation," *IEEE Trans. Power Syst.*, vol. 3, no. 3, pp. 830–836, Aug. 1988.
[26] J. Zhang, G. Welch, and G. Bishop, "Observability and estimation uncertainty analysis for PMU placement alternatives," in *Proc. North Amer. Power Symp.*, 2010, pp. 1–8.
[27] K. Zhu, L. Nordstrom, and L. Ekstam, "Application and analysis of optimum PMU placement methods with application to state estimation accuracy," in *Proc. IEEE Power & Energy Soc. Gen. Meeting*, 2009, pp. 1–7.
[28] M. Asprou and E. Kyriakides, "Optimal PMU placement for improving hybrid state estimator accuracy," in *Proc. IEEE PowerTech*, Trondheim, Norway, 2011, pp. 1–7.
[29] Q. Li, R. Negi, and M. Ilic, "Phasor measurement units placement for power system state estimation: A greedy approach," in *Proc. IEEE Power and Energy Soc. Gen. Meeting*, 2011, pp. 1–8.
[30] V. Kekatos and G. Giannakis, "A Convex relaxation approach to optimal placement of phasor measurement units," in *Proc. 4th IEEE Int. Workshop Computational Advances in Multi-Sensor Adaptive Process.*, 2011, pp. 145–148.
[31] Q. Li, T. Cui, Y. Weng, R. Negi, F. Franchetti, and M. Ilic, "An information-theoretic approach to PMU placement in electric power systems," *IEEE Trans. Smart Grid*, vol. 4, no. 1, pp. 445–456, Mar. 2013.
[32] N. Manousakis, G. Korres, and P. Georgilakis, "Taxonomy of PMU placement methodologies," *IEEE Trans. Power Syst.*, vol. 27, no. 2, pp. 1070–1077, May 2012.
[33] W. Yuill, A. Edwards, S. Chowdhury, and S. Chowdhury, "Optimal PMU placement: A comprehensive literature review," in *Proc. IEEE Power and Energy Soc. Gen. Meeting*, 2011, pp. 1–8.
[34] J. Lavaei and S. Low, "Zero duality gap in optimal power flow problem," *IEEE Trans. Power Systems*, vol. 27, no. 1, pp. 92–107, Feb. 2012.
[35] B. Stott and O. Alsaç, "Fast decoupled load flow," *IEEE Trans. Power App. Syst.*, vol. PAS-93, no. 3, pp. 859–869, May 1974.
[36] R. Nuqui and A. Phadke, "Phasor measurement unit placement techniques for complete and incomplete observability," *IEEE Trans. Power Del.*, vol. 20, no. 4, pp. 2381–2388, Oct. 2005.
[37] N. Abbasy and H. Ismail, "A unified approach for the optimal PMU location for power system state estimation," *IEEE Trans. Power Syst.*, vol. 24, no. 2, pp. 806–813, May 2009.
[38] X. Li, A. Scaglione, and T.-H. Chang, "A framework for phasor measurement placement in hybrid state estimation via Gauss-Newton," Tech. Rep. [Online]. Available: http://arxiv.org/pdf/1309.4911,
[39] X. Li and A. Scaglione, "Convergence and applications of a gossip-based Gauss-Newton algorithm," *IEEE Trans. Signal Process.*, vol. 61, no. 21, pp. 5231–5246, Nov. 2013.
[40] S. Kay, *Fundamentals of Statistical Signal Processing, Volume 1 and II: Estimation and Detection Theory*. Upper Saddle River, NJ, USA: Prentice-Hall PTR, 1998.
[41] S. Boyd and L. Vandenberghe, *Convex Optimization*. Cambridge, U.K.: Cambridge Univ, 2004.
[42] A. Charnes and W. Cooper, "Programming with linear fractional functionals," *Naval Research Logistics Quarterly*, vol. 9, no. 3–4, pp. 181–186, 1962.
[43] Z. Luo, W. Ma, A. So, Y. Ye, and S. Zhang, "Semidefinite relaxation of quadratic optimization problems," *IEEE Signal Process. Mag.*, vol. 27, no. 3, pp. 20–34, Mar. 2010.
[44] K. Martin, D. Hamai, M. Adamiak, S. Anderson, M. Begovic, G. Benmouyal, G. Brunello, J. Burger, J. Cai, and B. Dickerson *et al.*, "Exploring the IEEE Standard c37. 118-2005 Synchrophasors for Power Systems," *IEEE Trans. Power Del.*, vol. 23, no. 4, pp. 1805–1811, Oct. 2008.

Xiao Li (S'08) received the B.Eng. degree from Sun Yat-Sen (Zhongshan) University, China, in 2007, and the M.Phil. degree from the University of Hong Kong in 2009. He is currently working toward the Ph.D. degree at the University of California, Davis, CA, USA.

His research interests are in the theoretical and algorithmic studies in signal processing and optimizations, statistical learning and inferences for high-dimensional data, distributed optimizations and adaptive algorithms, as well as their applications in communications, networked systems, and smart grid.

Anna Scaglione (F'10) received the Laurea (M.Sc.) degree and Ph.D. degree from the University of Rome, "La Sapienza, " Rome, Italy, in 1995 and 1999, respectively.

She is currently a Professor with the Department of Electrical and Computer Engineering, University of California, Davis, CA, USA, which she joined in 2008. Prior to that, she joined Cornell University, Ithaca, NY, USA, in 2001, where became an Associate Professor in 2006. Prior to joining Cornell University, she was an Assistant Professor with the University of New Mexico from 2000 to 2001.

She served as Associate Editor for the IEEE TRANSACTIONS ON WIRELESS COMMUNICATIONS from 2002 to 2005, and serves since 2008 the Editorial Board of the IEEE TRANSACTIONS ON SIGNAL PROCESSING from 2008 to 2011, where she is Area Editor. Dr. Scaglione received the 2000 IEEE Signal Processing Transactions Best Paper Award the NSF Career Award in 2002 and she is co-recipient of the Ellersick Best Paper Award (MILCOM 2005) and the 2013 IEEE Donald G. Fink Prize Paper Award. Her expertise is in the broad area of signal processing for communication systems and networks. Her current research focuses on communication and wireless networks, sensors' systems for monitoring, control and energy management and network science.

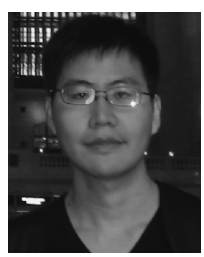

Tsung-Hui Chang (S'07–M'08) received the B.S. degree in electrical engineering and Ph.D. degree in communications engineering from the National Tsing Hua University, Hsinchu, Taiwan, in 2003 and 2008, respectively.

Since September 2012, he has been with the Department of Electronic and Computer Engineering, National Taiwan University of Science and Technology (NTUST), Taipei, Taiwan, as an Assistant Professor. Before joining NTUST, he held research positions with National Tsing Hua University, Hsinchu, Taiwan (2008–2011) and the University of California, Davis, CA (2011–2012). He was also a Visiting Scholar with the University of Minnesota, Twin Cities, MN, USA, the Chinese University of Hong Kong, and Xidian University, China. His research interests are widely in signal processing problems in wireless communications and smart grid, and convex optimization methods and its applications.

Authorized licensed use limited to: Washington State University. Downloaded on October 11,2022 at 04:27:01 UTC from IEEE Xplore. Restrictions apply.